A miniaturized TEM nanoindenter for studying material deformation *in situ*

2006 Meas. Sci. Technol. 17 1324

(http://iopscience.iop.org/0957-0233/17/6/006)

INSTITUTE OF PHYSICS PUBLISHING MEASUREMENT SCIENCE AND TECHNOLOGY

Meas. Sci. Technol. **17** (2006) 1324–1329 doi:10.1088/0957-0233/17/6/006

A miniaturized TEM nanoindenter for studying material deformation *in situ*

M S Bobji[1], C S Ramanujan[2], J B Pethica[2] and B J Inkson[3]

[1] Department of Mechanical Engineering, Indian Institute of Science, Bangalore 560 012, India
[2] Department of Materials, University of Oxford, Parks Road, Oxford OX1 3PH, UK
[3] Department of Engineering Materials, The University of Sheffield, Mappin Street, Sheffield S1 3JD, UK

Received 7 August 2005, in final form 14 February 2006
Published 2 May 2006
Online at stacks.iop.org/MST/17/1324

Abstract
A miniaturized nanoindenter system has been designed and fabricated to carry out localized *in situ* deformation studies in a high resolution transmission electron microscope (TEM). The coarse positioning is carried out with the help of small inertial drives so that the whole system could fit into the specimen holder of the JEOL 2010 microscope. The fine positioning is achieved with a piezoelectric tube and the force is measured with the help of a four bar flexible hinge spring element. The ability of the system to correlate the force–distance data with the events observed in TEM is demonstrated.

Keywords: *in situ* TEM, nanoindentation, deformation mechanisms, inertial sliders

1. Introduction

For many areas of nano-science, the physical processes which take place as materials come into contact at the nano-scale are extremely important to understand. Processes such as local bonding and deformation at nano-contact sites are particularly important for determining how nano-scale materials components degrade and wear, for example in micro- and nano-electromechanical systems devices (MEMS and NEMS) (Clemens *et al* 1999, Josell *et al* 1998, Mitchell *et al* 1997, Savader *et al* 1997, Siegel and Fougere 1995, Sproul 1996).

A number of experimental techniques such as nanoindentation and atomic force microscopy (AFM) have been very successful in determining local nano-scale mechanical properties (Pethica *et al* 1983); however these techniques lack a method of simultaneous observation of local microstructural changes during the mechanical test. More recent developments combining nano-scale contact and STM probes with *in situ* observation of microstructure by transmission electron microscopy have been very successful in beginning to combine local mechanical testing with independent real-time imaging of microstructural evolution (Kizuka *et al* 1997, Svensson *et al* 2003, Wall and Dahmen 1998).

Whilst real-time imaging of deformation under nano-scale contacts is very informative, it is essential to develop methods of determining the stress, and hence force, under the contact probe in order to relate deformation mechanisms to mechanical properties of nano-scale volumes of materials. This requires careful design of the entire nanopositioning/nanoindentation system, to ensure adequate stiffness of the entire nanoindentation mechanism and mechanical stability of the combined coarse plus fine nanopositioning mechanisms. With these factors in mind, a new nanoindentation system has been designed to fit inside a transmission electron microscope (TEM) with a three-axis inertial slider positioning system and a special spring capable of measuring force.

2. Nanoindenter design

A schematic of the instrument developed is shown in figure 1. It consists of a three-axis inertial slider (Pohl 1987, Bobji *et al* 2003) based coarse positioner that moves a four-quadrant piezoelectric tube used for generating fine motions. The force sensor spring that carries the indenter tip is mounted at the end of the tube piezo and is accommodated within the objective lens pole piece gap of the TEM. The whole nanopositioning mechanism fits inside the 10 mm bore of a side entry specimen

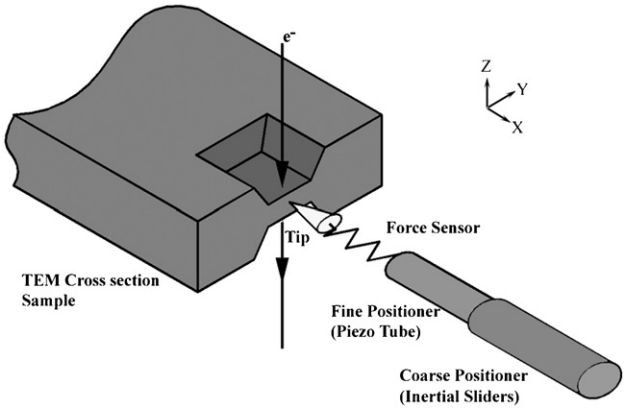

Figure 1. Schematic of the TEM nanoindenter. The indentation axis (x) is perpendicular to the optic axis (z) enabling the deformation to be observed in the transmission electron microscope.

holder that is compatible with JEOL 2010 and 3000 series microscopes. All the moving parts are within the vacuum and the instrument is sealed with an O-ring that also doubles up as a vibration isolator.

The specimen to be investigated is fixed rigidly onto the TEM specimen holder frame with an electron-transparent area at its edge perpendicular to the electron beam. The electron-transparent area is then indented perpendicular to the e-beam with a sharp tip which moves relative to the specimen and holder frame as shown schematically in figure 1. This specimen/tip geometry enables any plastic deformation resulting from the indentation to be imaged *in situ* by the e-beam. The sharp indenting tips, used initially, have been fabricated by electro-polishing tungsten wire, although any geometry tip that fits inside the microscope pole-piece gap can in principle be used.

2.1. Three-axis inertial drive coarse positioner

To be electron-transparent a typical metal such as Cu has to be thinner than 300 nm when the electrons are accelerated with a typical TEM voltage of 200 kV. In order to get the tip in the same plane as the electron-transparent area of the specimen (prior to indenting using fine motion generated by the tube piezo), the tip should be capable of being positioned in the range of a few mm using a coarse positioner with a resolution (step-size) better than 300 nm in at least two perpendicular axes (x and z in figure 1). Such a coarse positioner, which has to fit within a standard TEM holder and has excellent mechanical stability to prevent vibrations degrading the resolution of the electron microscope and indentation tests, has been achieved here using piezoelectrically driven stick–slip inertial sliders (Bobji *et al* 2003).

Inertial sliders (figure 2) have been used extensively in scanning probe microscopes (for example see Svensson *et al* (2003)). They have the inherent advantage of precision and compactness over other mechanical drives, especially when they are based on piezoelectric shear plates. Inertial sliders use simple drive electronics and do not require precision-machined parts. Importantly, when not in operation they can act as stiff structural members, generating no vibration. A schematic of all the essential elements of an inertial drive

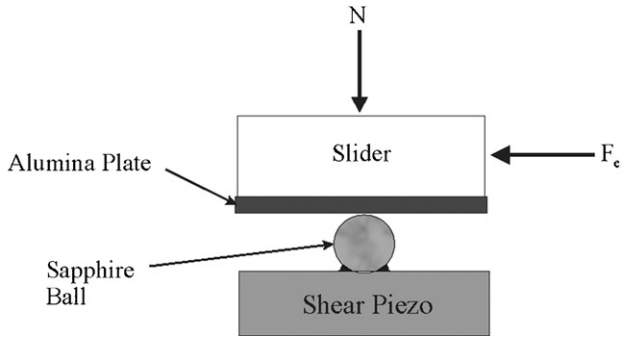

Figure 2. Schematic of the inertial slider. N is the force normal to the sapphire–alumina contact plane and F_e is the frictional force in the contact plane. The ball slips against the slider if the inertial and external forces are greater than the frictional force.

as used in our instrument is shown in figure 2. It consists of a contact between a 1 mm diameter sapphire ball and an alumina plate attached to the moving element, referred to as a slider. The stiffness of the drive comes from the friction force at the contact (F_e) and can be tuned by adjusting the normal force N. We achieve this adjustment of N by means of a spring attached to the slider (see figure 3). A shear piezoelectric plate ($5 \times 5 \times 0.75$ mm^3) is used for generating the displacements. When a positive voltage of 300 V is applied between the top and bottom surfaces of the shear piezoelectric plate the top surface displaces by 275 nm. The velocity and acceleration with which the sapphire ball attached to the top surface moves can be adjusted by controlling the waveform of the voltage applied to the shear piezo. For example, a linear rise in voltage will give a constant velocity displacement of the ball and a quadratic rise will give a constant acceleration.

To achieve forward motion of the inertial slider the voltage waveform is adjusted such that the total force (external force + inertial force) acting on the slider is at first less than the frictional force at the contact. The ball and the alumina plate 'stick' together and move as one unit. The piezo voltage is then dropped sharply to zero within 2 μs. By controlling the mass of the slider to make the inertial force exceed the frictional force, the ball slides against the alumina plate and the sapphire ball is brought back to its original position with a very high acceleration. This process results in a net forward motion of the slider. By repeating this cycle, the slider can be moved over a long range. The reverse motion is achieved by applying the same waveform to the bottom surface of the piezoelectric plate.

Figure 3 shows the three-axis (Cartesian axes x, y and z) inertial drive positioner that has been used. Reducing the size to fit inside a TEM holder shaft proved to be a big design challenge. The elastic deformation of the drive parts, especially the piezoelectric elements, the mating glue and the sapphire balls, plays an important role in the performance of the inertial drives. We used a numerical solution of the equation of motion (for example see Chang and Li (1999)) to optimize the design. Very thin layers of vacuum compatible conductive epoxy were used as the glue, and a special holder was designed to attach the balls on to the piezoelectric plates. In order to reduce the effect of the external forces (friction at

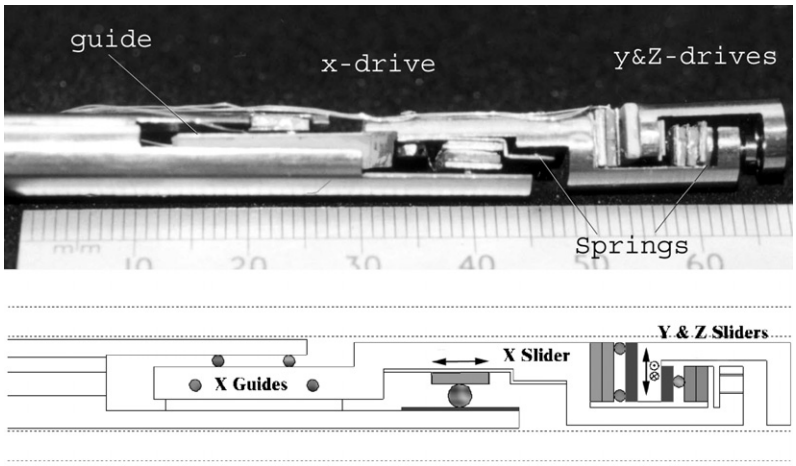

Figure 3. Image and schematic of the three-axis coarse positioner. The springs help to adjust the frictional force at the ball–plate interfaces.

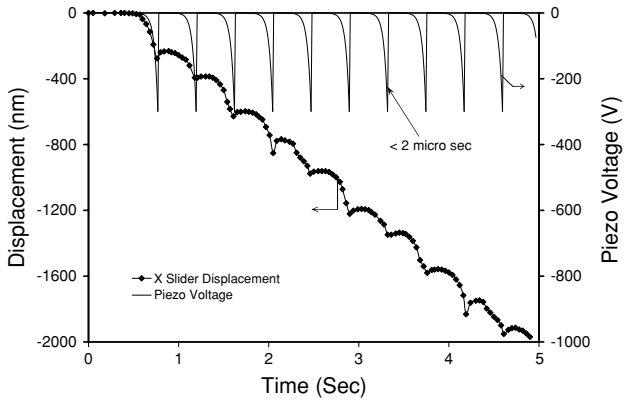

Figure 4. Performance of the coarse X-slider. The continuous line shows the waveform applied to the piezo. The resulting slider displacement (filled diamonds) is measured with the help of a heterodyne interferometer.

the supporting contacts—F_e in figure 2), two drive elements have been used for each of the three perpendicular axes, and all four supporting balls for y and z drives are active.

Figure 4 shows the performance of the X-slider for an exponential rise voltage followed by a sharp return applied to the piezoelectric plate. The movement of the slider is measured with a heterodyne interferometer. It can be seen that the slider moves forward during exponential voltage increase and there is a small backward displacement during the sharp voltage drop for every cycle. The backward displacement could be due to the recovery of the drive parts from the elastic deformation due to the frictional and external forces. At very low-frictional forces (the minimum is just higher than the external forces), the step size is almost 275 nm per voltage loop corresponding to the free displacement of the piezoelectric element for the maximum voltage applied. At very high frictional forces, the slider just moved back and forth without slipping, giving no net displacement. We could thus optimize the friction force for the best compromise between the net step size per voltage loop (controlling the speed) and the load that the drive can support as a structure when not in operation. We measured that our drive can withstand up to 22 g load without slipping in the x-axis, which is very high compared to the expected maximum indentation load of a few tens of milligrams.

2.2. *Three-axis fine positioner*

In the developed nanopositioning stage, a four quadrant piezoelectric tube of diameter 3.13 mm and length 50 mm is used to generate fine x, y and z motions of the tip. The piezoelectric tube has a maximum range of 2 μm along the long axis of the holder (x-axis, figure 1), and 20 μm in the other two perpendicular axes (y and z, figure 1). The magnitude of the fine positioning step can be down to 0.3 Å.

The longer range and the finer resolution of the developed inertial drive coarse positioner (section 2.1) compared to other nanopositioning holders (Kizuka *et al* 1997, Wall and Dahmen 1998) means that the desired fine nanopositioning (indentation) motion can be generated by very small electric fields and the fine tube piezo operated within the central 10% of its possible displacement range. As a result of working at low piezo voltages (typically $\pm$20 V and mounting the piezo at 10 mm distance from the electron beam) we did not find any appreciable distortion in the TEM images even at very high magnification whilst moving the tip. Working at low voltages improves the linearity of the voltage–displacement response of the piezoelectric element, and reduces the likelihood of its depolarization. The purity of x, y and z motions of the piezoelectric tube can be calibrated in the TEM by observing the free motion of the tip with applied voltage.

2.3. *Force sensor*

The force sensor is shown in figure 5. It has a spring element which uses a four bar mechanism based on flexible elastic hinges (Nishimura 1991, Bobji 1999) that ensures a linear motion of the indenter in the plane of the sensor. Measurement of the deflection of the force sensor is obtained from the TEM images. In figure 5, the hinges A, B, C and D form the basis of a four bar mechanism. Link AB is attached to the piezoelectric tube and the tip is mounted on link CD. During indentation link AB moves by δ_p, the amount dictated by the motion generated by the piezoelectric tube, while link CD moves by δ_t which depends on the indentation forces. If k is the stiffness of the force sensor then the force F is given by

$$F = k(\delta_p - \delta_t). \quad (1)$$

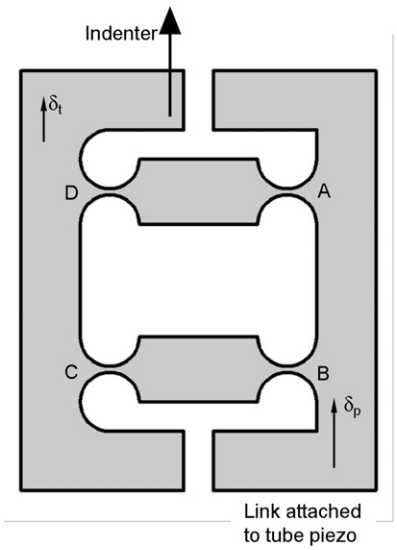

Figure 5. Schematic of the nanoindenter force sensor based on four flexible hinges marked as A–D. These hinges form a four bar mechanism that ensures the indenter moves in a straight line with respect to the piezo.

The stiffness k of the force sensor is measured by indenting a cantilever of known stiffness instead of the sample in a separate set-up outside the TEM. The displacement of the cantilever is measured with a heterodyne interferometer. The stiffness of the force sensor can be varied by varying the web thickness of the elastic hinges. The sensor was fabricated out of 0.25 mm thick Cu–Be plate by photo-etching, with the photo mask applied to both sides. The typical stiffness of the indenter used is about 1700 N m^{-1}. This means that, depending on the TEM magnification at which the indentation is carried out, forces as small as 0.1 μN can be measured.

2.4. Tip and sample preparation

The tips used in the initial studies were fabricated by etching electrochemically a tungsten wire of 0.1 mm diameter in a 2M NaOH solution using a graphite electrode. The tips are fixed with epoxy glue onto a groove in the force sensor plate. Initial samples were prepared using a focused ion-beam microscope. Samples were mechanically pre-thinned to about 100 μm. Electron-transparent regions, typically 20 $\times$ 5 $\times$ 0.3 μm^3 in size, were subsequently machined into the specimen edge.

3. Performance of the nanoindentation holder

The indenting tip is positioned at a distance of 2 mm away from the specimen in the x–y plane (figure 1) when loading the holder into the TEM. TEM imaging at low magnification is then used to get the tip closer to the specimen along the x- and y-axes using the coarse positioning drive. In order to make contact and indent the specimen, the tip should be positioned in the vertical z-axis (figure 1) to be as close as possible to the centre of the electron-transparent region of the specimen. We achieved this, as elsewhere (Kizuka *et al* 1997), by the observation and analysis of the Fresnel focus fringes at the edges of the specimen and tip at a magnification of 100 000$\times$ or more. These Fresnel fringes have also been used to check (and correct if necessary) that the axis of motion of the tip during fine positioning is in the x–y plane of focus.

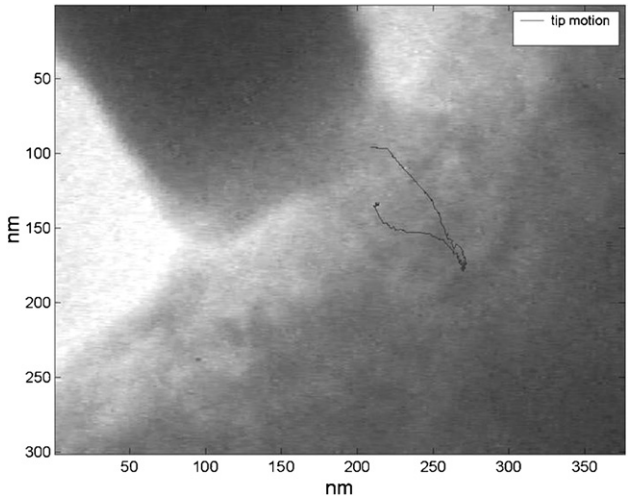

Figure 6. TEM image showing the copper sample being indented by a tungsten tip. The curve at the centre of the image shows the trajectory of the tip during the loading–hold–unloading cycle.

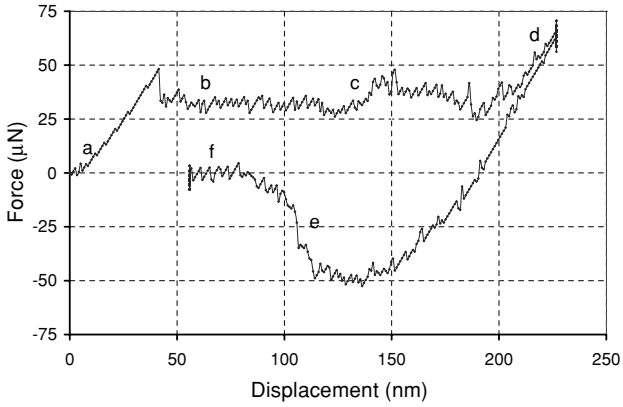

Figure 7. The load–displacement curve obtained from a series of TEM images. While unloading there is an attractive force on the indenter corresponding to the material being pulled out of the sample—stages e and f.

The relative vibration of the tip with respect to the TEM column and the specimen has been observed to be less than 0.1 nm, which is sufficiently stable to enable the holder to be used for high-resolution (atomic) imaging. The main source of vibration has been found to be the cables that connect the piezoelectric drives to the external control electronics.

Figure 6 shows an image of an electro-polished tungsten tip in the process of indenting a fractured copper surface. The rate of indentation is about 1 nm s^{-1}. The indentation is recorded onto SVHS videotape at 25 frames s^{-1} via an analogue TV camera. The continuous line in the image is the trajectory in the x–y image plane taken by the tip with respect to the sample during the loading, hold and unloading cycle. The trajectory is obtained from a series of digitized consecutive video images which have been aligned (and compensated for drift) by cross-correlation. The hysteresis between the loading and unloading trajectories is due to a combination of

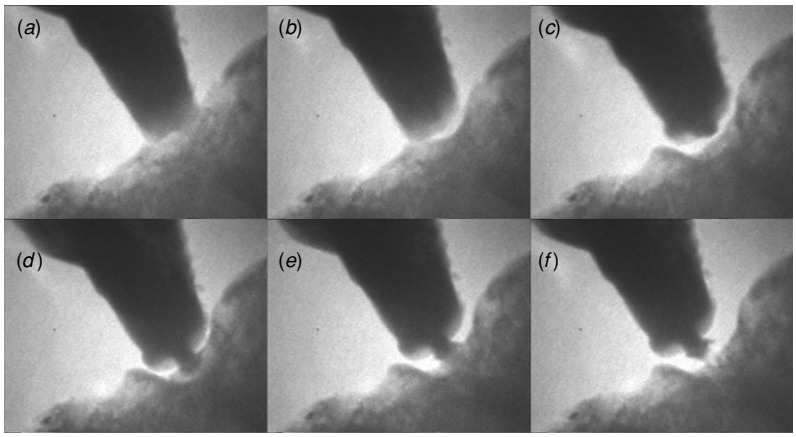

Figure 8. TEM images showing different stages during indentation of a fractured copper surface. The stages, (a)–(f), represent distinct events taking place in the load–displacement curve as marked in figure 7. Each image is of size 1500×1000 nm^2

the hysteresis of the piezoelectric tube used to generate the motion and because the axis of the indenter motion is inclined to the specimen edge. The deformation of the (non-uniform) specimen is also likely to be asymmetric.

The deflection of the force sensor ($\delta_p - \delta_t$) during the indentation is obtained by subtracting the trajectory taken by the tip with respect to the sample (δ_t) from the trajectory of the tip (δ_p) measured far away from the sample for the same voltage applied to the piezoelectric tube. The force on the indenter can then be obtained from equation (1). The stiffness of the force sensor was obtained in a set-up outside the TEM. The stiffness of the force sensor used was about 1700 N m^{-1}.

Figure 7 shows the resulting load–displacement curve of the indent. As soon as the indenter comes in contact with the copper specimen, the load increases with the displacement upto about a penetration depth of 40 nm. Then there is a sudden decrease in the load (point b in figure 7). Figure 8 shows the TEM still images obtained from the recorded movie corresponding to various positions (a–f) in the load–displacement curve. It can be seen that at point b there is some material transfer from the copper sample to the tip. By increasing the penetration further the load remains constant upto point c. At c, there is further transfer of material. As the penetration is further increased the contact occurs between the sample and the transferred material. While unloading, the whole indented region relaxes first and as the tip is retracted further a bridge-like structure (figure 8(e)) is formed between the tip and the sample. The load on the tip becomes tensile (e) as this structure is stretched before the contact is finally broken (f).

In this particular indentation sequence no dislocation-related activity was observed in the copper specimen. It may be that some highly localized dislocation activity occurred close to the indenter tip but for this particular sample was simply not resolved. Dislocations may not be resolved due to a number of factors including (i) if the local crystal orientation and diffraction condition used to observe the indentation in TEM did not produce sufficient contrast, (ii) if any dislocation segments generated were very short and localized in the severely strained zone (where crystal orientation and thus diffraction conditions differ from the surrounding sample) and (iii) if possible surface damage from FIB-machining of the sample masked defect contrast. Although discrete dislocation activity was not observed in figure 7, the sample deformed plastically, with local strain inducing fracture, leading to material transfer from the sample to the tip. Dislocation activity has been observed in later experiments when indenting a twinned region of Cu–Be alloy (Bobji *et al* 2005), where roughness at the nm level on a tip caused a dislocation cluster to be generated.

4. Conclusions

An *in situ* TEM nanoindenter capable of creating local deformation while simultaneously observing the deformation mechanics has been designed and fabricated. It has a high stiffness of 1.7 kN m^{-1} and can still measure small forces of the order of 1 μN. This nanoindenter has a high precision spatial positioning inertial drive for coarse drive (<300 nm), with large 5 mm range. This results in a relatively low-voltage operation of the fine positioner. The compact design has better stability, resulting in a very low relative vibration between the tip and the sample and hence is capable of *in situ* imaging at high resolution. Depending on the system being studied, it is possible to select the force sensor with the right stiffness to achieve the best force resolution. Such a holder can be used to measure the forces associated with various sub-surface deformation events during indentation inside a TEM (Bobji *et al* 2005).

Acknowledgments

This project was funded by the EPSRC under grant GR/M89690. The authors express their gratitude to John Stead for technical assistance in building the holder, Ron Doole for discussions on design, Cyril Band for fabrication of the force sensor, Ahmet Oral for electronics and software support and Dr E Stach (LBL, Berkeley) for helpful discussions on TEM nanoindentation.

References

Bobji M S 1999 Studies on depth sensing indention *PhD Thesis* Indian Institute of Science, Bangalore, India

Bobji M S, Pethica J B and Inkson B J 2005 Indentation mechanics of Cu–Be quantified by an *in-situ* TEM mechanical probe *J. Mater. Res.* **20** 2726–32

Bobji M S, Ramanujan C S, Doole R C, Pethica J B and Inkson B J 2003 *Materials Research Society Symp. Proc. (2003) (Mechanical Properties Derived from Nanostructuring Materials,* vol 778*)* pp 105–10

Chang S H and Li S S 1999 A high resolution long travel friction-drive micropositioner with programmable step size *Rev. Sci. Instrum.* **70** 2776–82

Clemens B M, Kung H and Barnett S A 1999 Structure and strength of multilayers *MRS Bull.* **24** 20–6

Josell D, van Heerden D, Read D, Bonevich J and Shechtman D 1998 Tensile testing low density multilayers: aluminum/titanium *J. Mater. Res.* **13** 2902–9

Kizuka T, Yamada K, Deguchi S, Naruse M and Tanaka N 1997 Cross-sectional time-resolved high-resolution transmission electron microscopy of atomic-scale contact and noncontact-type scannings on gold surfaces *Phys. Rev.* B **55** R7398–401

Mitchell T E, Lu Y C, Griffin A J, Natasi M and Kung H 1997 Structure and mechanical properties of copper/niobium multilayers *J. Am. Ceram. Soc.* **80** 1673–6

Nishimura K 1991 A spring-guided micropositioner with linearized subnanometer resolution *Rev. Sci. Instrum.* **62** 2004–7

Pethica J B, Hutchings R and Oliver W C 1983 Hardness measurement at penetration depths as small as 20 nm *Phil. Mag.* A **48** 593–606

Pohl D W 1987 Dynamic piezoelectric translation devices *Rev. Sci. Instrum.* **58** 54–7

Savader J B, Scanlon M R, Cammarata R C, Smith D T and Hayzelden C 1997 Nanoindentation study of sputtered nanocrystalline iron thin films *Scr. Mater.* **36** 29–34

Siegel R W and Fougere G E 1995 Mechanical properties of nanophase metals *Nanostruct. Mater.* **6** 205–16

Sproul W D 1996 New routes in the preparation of mechanically hard films *Science* **273** 889–92

Svensson K, Jompol Y, Olin H and Olsson E 2003 Compact design of a transmission electron microscope-scanning tunneling microscope holder with three-dimensional coarse motion *Rev. Sci. Instrum.* **74** 4945–7

Wall M A and Dahmen U 1998 An *in situ* nanoindentation specimen holder for a high voltage transmission electron microscope *Microsc. Res. Tech.* **42** 248–54